EurJIC

European Journal of Inorganic Chemistry

Chemistry Europe

European Chemical Societies Publishing

# Accepted Article

**Title:** New Variants of (110)-Oriented Layered Lead Bromide Perovskites, Templated by Formamidinium or Pyrazolium

**Authors:** YUanyuan Guo, Clement Elliott, Jason McNulty, David Cordes, Alexandra Slawin, and Philip Lightfoot



**To be cited as:** *Eur. J. Inorg. Chem.* 10.1002/ejic.202100433

**Link to VoR:** https://doi.org/10.1002/ejic.202100433

WILEY-VCH

10.1002/ejic.202100433

# New Variants of (110)-Oriented Layered Lead Bromide Perovskites, Templated by Formamidinium or Pyrazolium

Dr Yuan-Yuan Guo, Mr Clement Elliott, Dr Jason A. McNulty, Dr David B. Cordes, Prof. Dr Alexandra M. Z. Slawin and Prof. Dr Philip Lightfoot*

School of Chemistry and EaStChem, University of St Andrews, St Andrews, KY16 9ST, United Kingdom

*E-mail: pl@st-andrews.ac.uk; https://www.st-andrews.ac.uk/chemistry/people/pl



## Abstract

Four new hybrid lead(II) halide perovskites, γ-$(FA)_2PbBr_4$, $(FA)_{1.5}(AA)_{0.5}PbBr_4$, (PY)(GA)$PbBr_4$ and (PY)(TZ)$PbBr_4$ ((FA) = formamidinium, (AA) = acetamidinium, (PY) = pyrazolium, (GA) = guanidinium and (TZ) = 1,2,3-triazolium), adopt (110)-oriented layered perovskite structures. While (PY) is found to template the formation of 'conventional' (110)-oriented structure types (i.e. containing staggered $[PbBr_4]_\infty$ layers), (FA) is shown to facilitate formation of much less common variants based 3:1 ordering of the interlayer species or 3 × 2 step-like corrugation of the perovskite-like layers themselves.

## Introduction

Hybrid layered perovskites, particularly lead(II) halide perovskites (LHPs), play a significant role in functional materials due to their structural flexibility and attractive chemical and physical properties. Their impressive performances in photophysical and electronic applications such as solar cells[1,2] and light-emitting devices[3] are well documented. Very small molecular cations, such as methylammonium (MA) and formamidinium (FA) are well-known to be able to template the formation of traditional 3D hybrid perovskites of composition $APbX_3$. The FA-containing materials can show remarkably improved performance for optoelectronic devices. $FAPbI_3$, for instance, displays a much broader absorption spectrum for visible light than its methylammonium counterpart ($MAPbI_3$) and demonstrates a power conversion efficiency of over 20% in photovoltaic devices.[4,5] $FAPbBr_3$, also exhibits a better stability and high quantum yield of up to 85% in highly monodisperse nanocrystals.[6] However, it is also

recognised that FA can template the formation of alternative lead halide structure types, particularly 2D layered LHPs. For example, since FA is sufficiently small to occupy the A-site in a 3D perovskite, it can also be used as a 'perovskitiser' to template the formation of Ruddlesden-Popper-like 2D perovskites of generic compositions $(A)_m(FA)_{n-1}Pb_nX_{3n+1}$ ($m$ = 1,2; $n$ = 2,3,4…) where FA occupies exclusively the perovskite-like A-site rather than the larger, more flexible interlayer site.[7,8] More intriguingly, FA has also been shown to encourage formation of the much less common "(110)-cut" layered perovskite structure. Thus, both (HEA)(FA)$PbBr_4$[9] (HEA = hydroxyethylammonium) and (FA)(GA)$PbI_4$[10] (GA = guanidinium) have been reported to adopt (110)-like LHP structures. Very recently, two polymorphs of $FA_2PbBr_4$ have also been shown to adopt (110)-cut structure types, differing in the degree of relative staggering of the $[PbBr_4]_\infty$ layers.[11] It should be noted that compositions of the type $APbBr_4$, $A_2PbBr_4$ or $AA'PbBr_4$ have, in principle, a choice between adopting (100)-cut structure types (i.e. Ruddlesden-Popper or Dion-Jacobson families) or the (110)-cut family. A recent comprehensive review of the (100)-cut families reported more than 250 examples,[12] whereas recent works, including an on-line database,[13] suggest only around 20 examples of the (110)-cut family. Moreover, it has been noted that (110)-derived materials can offer particularly useful physical properties, such as broadband emission, due to their often higher degrees of distortion of the inorganic layers and greater degree of electronic confinement.[14] Targeted or exploratory studies aimed at extending the (110)-cut family are therefore important.

In our recent work[15,16] we have been exploring the use of small, rigid disc-like amines to target (110)-cut LHPs. For example, the compositions (IM)(GA)$PbBr_4$ (IM = imidazolium), (1,2,4-TZ)(GA)$PbBr_4$ (1,2,4-TZ = 1,2,4-triazolium) and $(AA)_2PbBr_4$ (AA = acetamidinium), all show variants of the 'standard' (110)-cut structure types, originally reported in purely inorganic systems, such as $BiReO_4$[17] or $NdBaScO_4$[18] (Figure 1). There are a handful of examples of (110)-derived compositions in hybrid systems with differing inorganic-layer architectures, such as extended "$n \times n$" or "$n \times m$" step-like structures[10,19–21] or "eclipsed" layers[11,22] which may lead to 3:1 ordering of the interlayer species (Figure 1). In addition to the further exploration of small, rigid cyclic amines to template such systems, the use of FA in related systems is clearly a worthy avenue. In this paper we extend our study of disc-shaped amines to include pyrazolium (PY) and 1,2,3-triazolium (TZ), and also report new structural variants based on FA.

## Results and Discussion

*Crystal structures of γ-$(FA)_2PbBr_4$ and $(FA)_{1.5}(AA)_{0.5}PbBr_4$*

Crystal data for each compound are reported in Table 1. As stated above, two polymorphs of $(FA)_2PbBr_4$, based on the (110)-cut layered perovskite type, have recently been reported. Remarkably, under the synthetic conditions used here, a new polymorph of $(FA)_2PbBr_4$, now designated γ-$(FA)_2PbBr_4$, is isolated. Unlike the two recently reported polymorphs, which have 'staggered' and 'eclipsed' "2 × 2" (110)-cut structures (Figure 1), the present polymorph adopts a "3 × 2" arrangement of the inorganic layers (Figure 2). There are three distinct Pb sites and six different FA moieties. As far as we are aware, there is only one previously reported example of this type of "3 × 2" $[PbX_4]_\infty$ layer architecture: this occurs in $(FA)(GA)PbI_4$.[10] In that case the unit cell metrics are similar (also a $Z$ = 12 structure) but the symmetry is higher ($C2/c$) leading to only two distinct Pb sites. In each case, however, the 'central' Pb-centred octahedron, which has only *trans*-shared vertices (Pb(1) in the present case), is significantly less distorted than the two *cis*-shared octahedra (Table 2). There is a complex network of H-bonds linking the FA moieties to the framework (see ESI). Fateev *et al.*[11] crystallised their two distinct polymorphs of $(FA)_2PbBr_4$ from DMF solution, and suggested that the process is kinetically controlled, with the thermodynamic stability of the two polymorphs being similar. In our case, the distinctly different synthetic conditions (moderate heating in conc. HBr) are apparently favourable to the isolation of the γ polymorph, though calculations would be of interest to further explore the relative stabilities of the three polymorphs.

10.1002/ejic.202100433

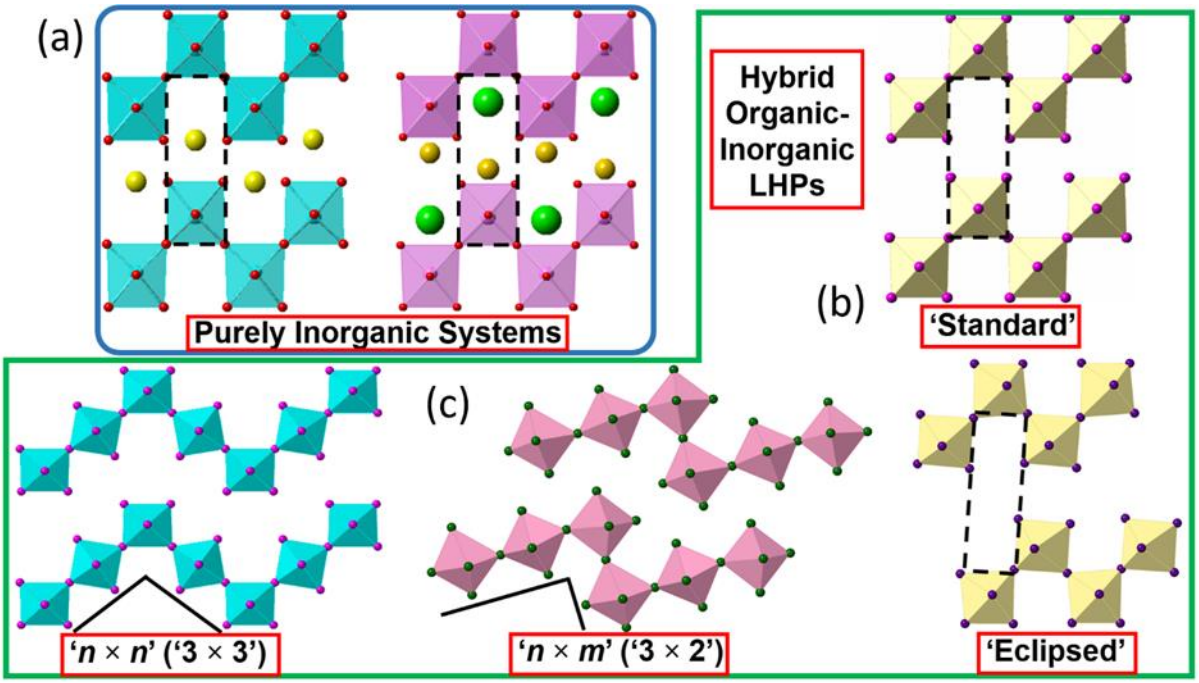


**Figure 1.** Schematics of the crystal structures of (110)-type layered perovskites (a) aristotype $ABX_4$ structure (left) and $AA'BX_4$ (right). (b) 'standard' and 'eclipsed' $[BX_4]_\infty$ layers observed in hybrid systems and (c) "3 × 3" and "3 × 2" step-like structures.

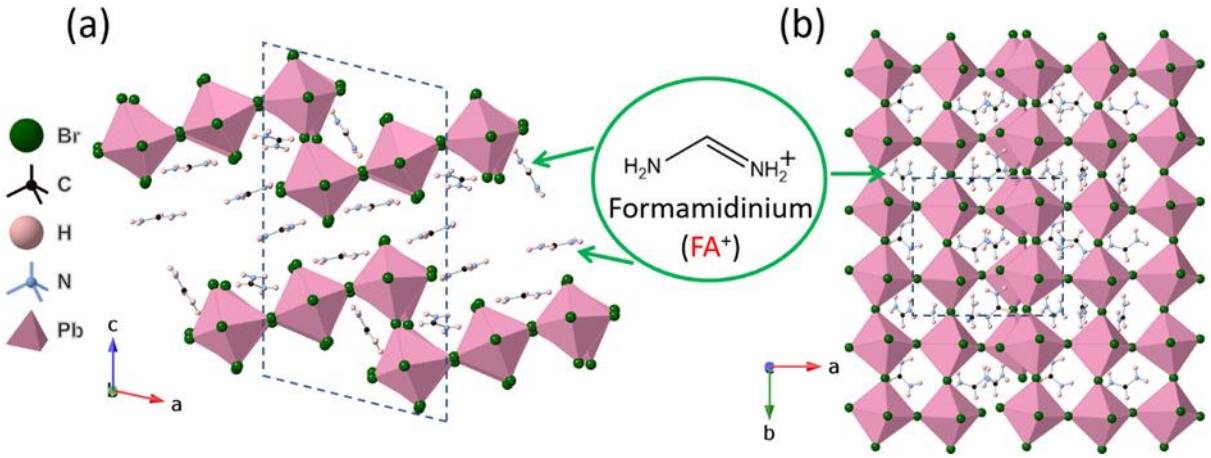


**Figure 2.** Crystal structure of γ-$(FA)_2PbBr_4$ (a) parallel to the inorganic layers and (b) perpendicular to the layers.

$(FA)_{1.5}(AA)_{0.5}PbBr_4$ adopts an eclipsed "2 × 2" (110)-cut structure type (Figure 3). There are only two previously known examples of this unusual eclipsed structure type: Fateev's triclinic $(FA)_2PbBr_4$ polymorph referred to above and the tin iodide, $(GA)_{1.5}(MI)_{0.5}SnI_4$ (MI = 1-methylimidazolium), previously reported by our group.[22] A 3:1 ordering of the molecular

cations exists in the present case, which can be related to that in $(GA)_{1.5}(MI)_{0.5}SnI_4$. In that case, the smaller GA moiety occupies the 'intralayer' perovskite-like site. In the present case, this position is preferable for the smaller of the two cations (FA), which forces the AA moiety to the alternate interlayer site. It can be expected that GA and AA are about the same size, though they obviously differ in H-bonding opportunities. We note that the unit cells of the family of "2 × 2" (110)-cut structures typically have one axis of ~ 6 Å (perpendicular to the corrugation direction), one of ~ 9 Å (along the corrugation direction) and one variable, depending on the interlayer species.[16] In the present case, the *a*-axis (perpendicular to the corrugation) is doubled due to out-of-phase octahedral tilting along *a*, with co-operative ordering of the organic moieties. A similar situation occurs in the two previously known examples. Comparison can also be made to the two previously mentioned cases of (110)-like systems containing combinations of FA and another organic cation, *viz.*, $(HEA)(FA)PbBr_4$[9] and $(FA)(GA)PbI_4$.[10] The former adopts the more standard staggered "2 × 2" structure, with the larger HEA cation occupying the intralayer site, whereas the latter adopts the "3 × 2" structure discussed above. Occupation of the intralayer site in $(HEA)(FA)PbBr_4$ by the larger HEA is perhaps surprising, but this was suggested to be related to the conformational flexibility of the HEA chain and the enhanced H-bonding opportunities of the -OH moiety.[9] The cation site preferences here, and the range of species that might stabilise this structure type are therefore difficult to rationalise at the moment, and are worthy of further study. So far, our attempts to prepare the tin iodide of $(FA)_{1.5}(AA)_{0.5}PbBr_4$ have been unsuccessful.

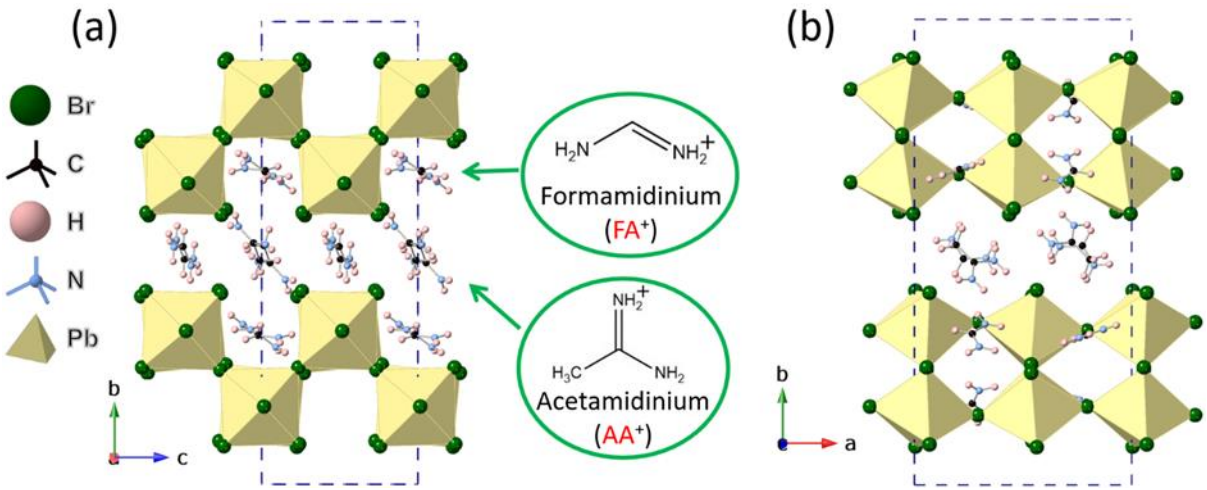


**Figure 3**. Two views of the crystal structure of $(FA)_{1.5}(AA)_{0.5}PbBr_4$ parallel to the inorganic layers (a) along the *a*-axis and (b) along the *c*-axis.

*Crystal structures of (PY)(GA)PbBr$_4$ and (PY)(TZ)PbBr$_4$*

Neither PY nor TZ have been previously incorporated into (110)-cut LHPs. In fact, we can see no previous examples of incorporation of TZ into any hybrid lead halides, although we note that 1,2,4-TZ) has been employed previously by our group.[15,16,22,23] A more complex derivative of PY (2-(2-aminoethyl)pyrazolium) has been incorporated into LHPs, to produce an APbX$_4$ composition, but this has the much more common (100)-cut structure type.[24] In addition, there are examples of PY incorporation into perovskite-related halides of manganese and cadmium.[25] The specific motivation for studying the combination of PY and GA here was to compare to our previous study of (IM)(GA)PbBr$_4$ and (1,2,4-TZ)(GA)PbBr$_4$,[15] both of which produce staggered "2 × 2" (110)-cut structures, but intriguingly differ in the ordering of the two organic cations. The crystal structure of (PY)(GA)PbBr$_4$ is shown in Figure 4.

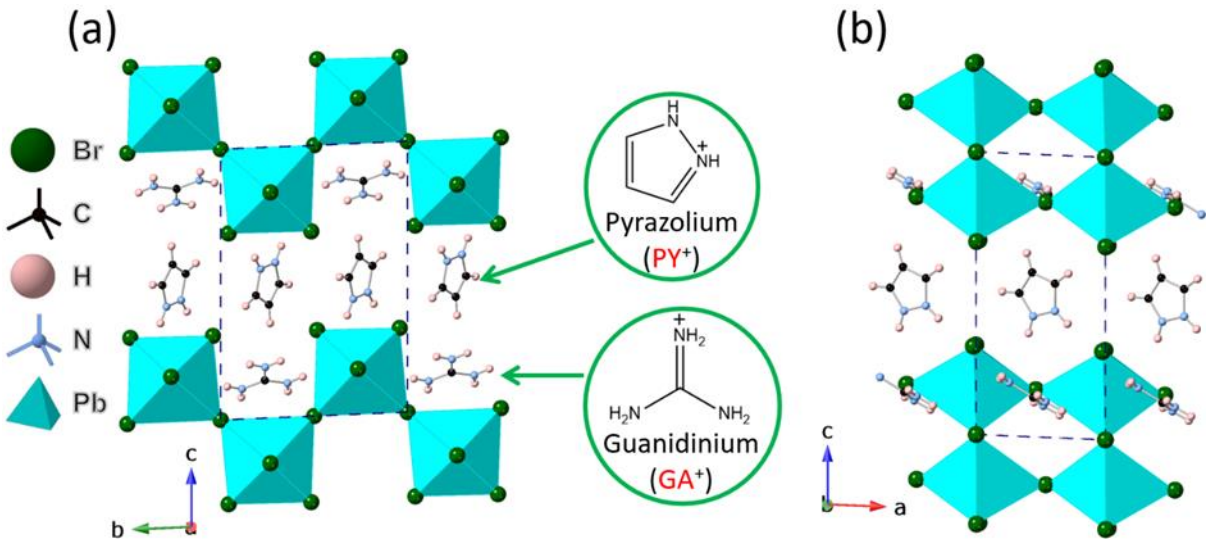


**Figure 4.** Two views of the crystal structure of (PY)(GA)PbBr$_4$ parallel to the inorganic layers (a) along the *a*-axis and (b) along the *b*-axis.

The unit cell axes follow the expected trend for this structure type, *viz*. ~ 6 Å (perpendicular to the corrugation direction) and ~ 9 Å (along the corrugation direction).[16] In this case, the unit cell metrics have a close similarity to those of (IM)(GA)PbBr$_4$; both crystallise in $P\bar{1}$ and may be regarded as isostructural. Indeed, closer inspection of (PY)(GA)PbBr$_4$ reveals that GA occupies the intralayer site, analogous to that in (IM)(GA)PbBr$_4$, and correspondingly PY occupies the interlayer site (like IM). Since the effective ionic sizes are about the same for the four species GA, IM, 1,2,4-TZ and PY, the contrasting behaviour in (1,2,4-TZ)(GA)PbBr$_4$[15] was discussed in terms of subtle preferences in H-bonding opportunities between the two different organic moieties. In fact, we identified a cooperative inter-molecular (GA---TZ) H-

bond in (1,2,4-TZ)(GA)$PbBr_4$ which was proposed to help stabilise the observed cation ordering pattern. This feature depends critically on the availability of the H-bond acceptor on 1,2,4-TZ. In contrast, although the species IM, PY and TZ are chemically very similar, only TZ has an unprotonated N atom available, and this difference appears to be the driving force for the isostructurality of (PY)(GA)$PbBr_4$ and (IM)(GA)$PbBr_4$. The H-bonding environment around the GA is equivalent in the two, while that of around the cation in the interlayer site (PY or IM) differs due to the relative placement of the N atoms.

(PY)(TZ)$PbBr_4$ has been studied here in order to further expand the structural chemistry of this family of materials. As discussed above, in our previous work we identified (1,2,4-TZ)(GA)$PbBr_4$ as a "2 × 2" (110)-cut structure type; we also later reported (1,2,4-TZ)(IM)$PbBr_4$ as a "3 × 3" (110)-cut structure.[16] Employing 1,2,3-TZ and PY produces another distinct variant of the "2 × 2" (110)-cut structure type; the structure of (PY)(TZ)$PbBr_4$ is shown in Figure 5.

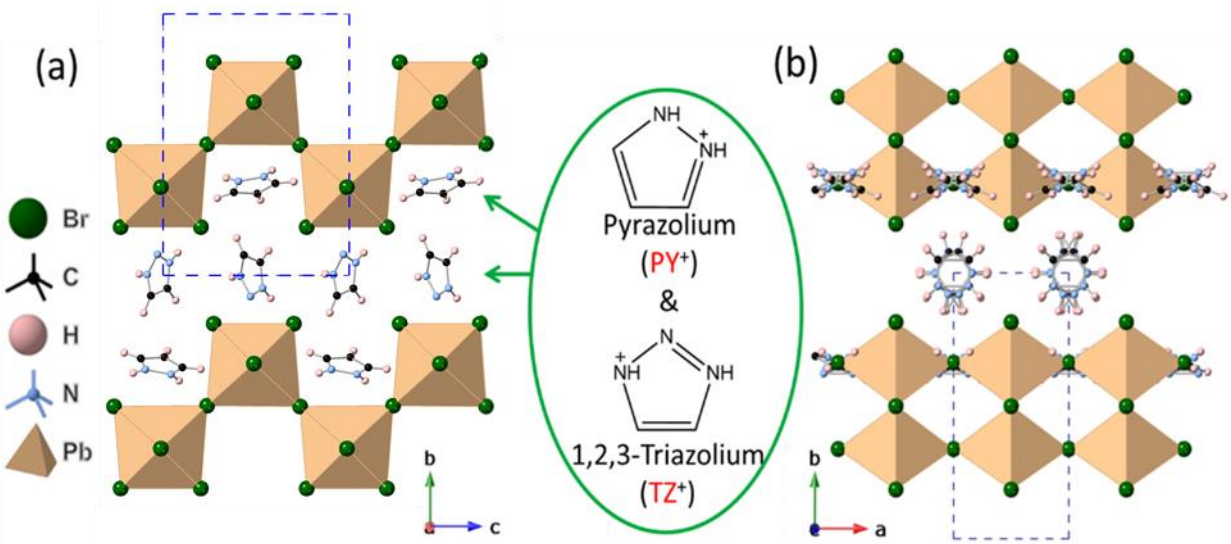


**Figure 5.** Two views of the crystal structure of (PY)(TZ)$PbBr_4$ parallel to the inorganic layers (a) along the *a*-axis and (b) along the *c*-axis.

Although the unit cell metrics again resemble those of (PY)(GA)$PbBr_4$ and (IM)(GA)$PbBr_4$ the symmetry in this case is higher, being orthorhombic. The best fit was determined in the polar space group $Pmc2_1$ rather than centrosymmetric, *Pmcm*, in order to accommodate more reasonable modelling of the organic cations. The Pb-centred octahedron lies on a mirror plane

($Z$ = 2) and although the refinement is robust the final model shows mixed occupancy of the cation sites by both organic moieties, complicated by symmetry-induced disorder of the individual cations. Hence, we are unable to distinguish any ordering pattern of the two cationic species, which are apparently too similar in size, shape and H-bonding preferences to adopt a well-ordered ground state. Comparison of the octahedral distortions in (PY)(GA)$PbBr_4$ and (PY)(TZ)$PbBr_4$ is useful to compare the difference in hydrogen-bonding behaviour between the two materials. Although the mean bond length distortion is similar for both ($\Delta d$ ~10.58 and 10.22, respectively), there is a considerable difference in the bond angle variance ($\sigma^2$ ~14.88 and 6.49, respectively). This may be attributable to the preferential ordering observed in (PY)(GA)$PbBr_4$, with PY favouring the interlayer site and GA the intralayer site, compared to the positional disorder of PY and TZ over both sites in (PY)(TZ)$PbBr_4$. Both TZ and PY are of a similar size and it is perhaps unsurprising that the interlayer distances of (PY)(GA)$PbBr_4$ (~4.84 Å) and (PY)(TZ)$PbBr_4$ (~4.91 Å) are of a correspondingly similar size.

*UV-Vis spectra*

UV–Vis absorbance spectra were carried out for both FA-containing samples (Figure 6) in order to compare with the previous $(FA)_2PbBr_4$ polymorphs. γ-$(FA)_2PbBr_4$ revealed features similar to previously reported (110)-cut layered LHPs, *viz.*, two separated absorption peaks.[10,15,26,27] That is, γ-$(FA)_2PbBr_4$ has two absorption peaks at 368 nm (3.37 eV) and 398 nm (3.12 eV). We suggest that the much weaker absorption features at longer wavelengths may be due to a trace amount of $FAPbBr^6$ impurity, which is unavoidable even using a large excess of $FA^+$ in the synthetic method used. There could also be some minor contribution from trace amounts of (100)-cut polymorphs. The Tauc-Plot reveals a band gap of 2.90 eV for γ-$(FA)_2PbBr_4$, as shown in the inset, Figure 6a. The band gap is similar to the very recently reported polymorphs (*t*-$(FA)_2PbBr_4$ and *m*-$(FA)_2PbBr_4$),[11] which have band gaps of 2.82 eV and 3.00 eV, respectively. Fateev *et al.* carried out a more detailed study of the band gaps in (110)-cut LHPs and found that *t*-$(FA)_2PbBr_4$ has the lowest band gap amongst (110)-cut lead bromides. This was ascribed to the very low intraoctahedral distortion parameter, $\Delta d \sim 3.9 \times 10^{-4}$, and short interlayer Br---Br contact, 4.15 Å. For comparison, the Δd parameters for γ-$(FA)_2PbBr_4$ are naturally much more varied due to the 3 × 2 structure, ranging from 0.9 - 29 × $10^{-4}$, but the shortest interlayer Br---Br contact is only 4.03 Å. In contrast, $(FA)_{1.5}(AA)_{0.5}PbBr_4$ displays a smaller band gap than any of the $(FA)_2PbBr_4$ polymorphs; a value of 2.62 eV is

observed (inset Figure 6b). Indeed, this is lower than any previously reported (110)-cut lead bromides.[11] It shows relatively small Δd parameters, in the range 4 - 6 × $10^{-4}$, but a shortest interlayer Br---Br contact that is much longer than the three $(FA)_2PbBr_4$ polymorphs, at 4.50 Å. The sharp excitonic absorption bands at ~ 400 nm for both γ-$(FA)_2PbBr_4$ and $(FA)_{1.5}(AA)_{0.5}PbBr_4$, can be attributed to the dielectric mismatch between organic and inorganic layers leads to strongly bound excitons.[26,28,29] The high energy bands at ~ 370 nm can be attributed to the combinations of charge transfer transitions within and between the inorganic and organic layers and higher order exciton transition energy levels.[30,31] The band gaps of the two compounds correspond to pale yellow and yellow colors for γ-$(FA)_2PbBr_4$ and $(FA)_{1.5}(AA)_{0.5}PbBr_4$, respectively (Figures 6c and 6d).

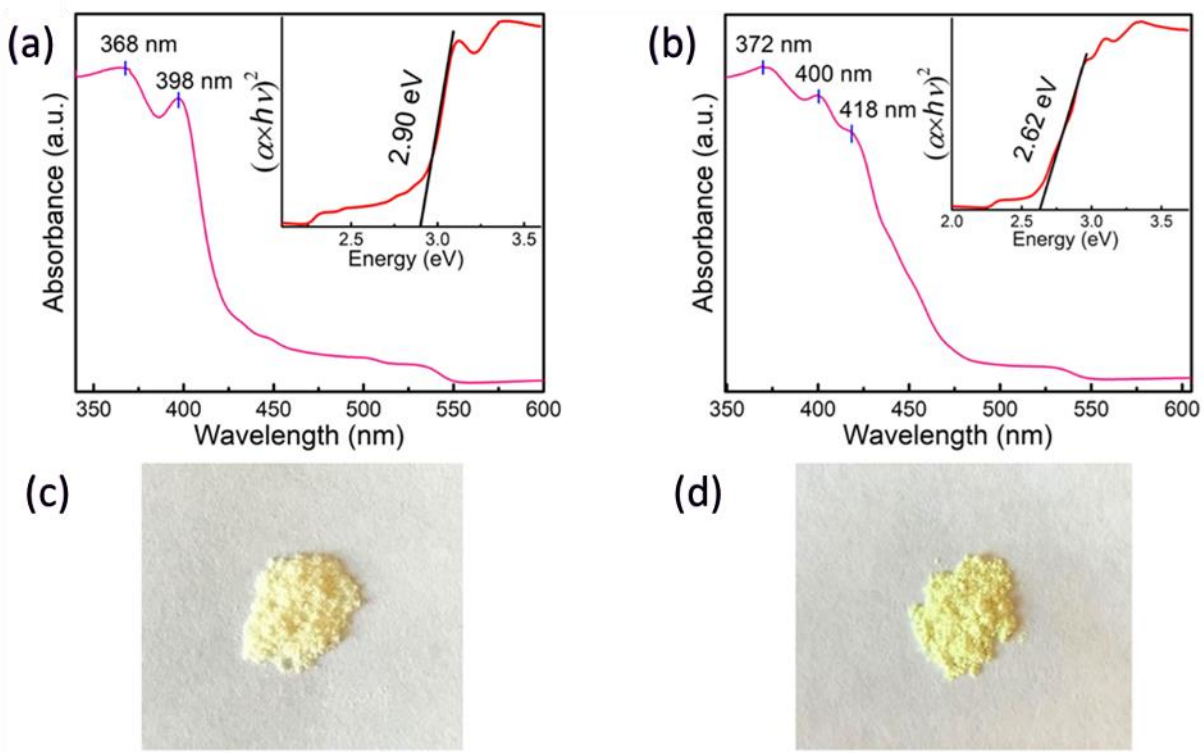


**Figure 6.** UV absorption spectra and Tauc-Plot (inset) of (a) γ-$(FA)_2PbBr_4$ and (b) $(FA)_{1.5}(AA)_{0.5}PbBr_4$. (c) and (d) show the colors of the two powdered samples γ-$(FA)_2PbBr_4$ and $(FA)_{1.5}(AA)_{0.5}PbBr_4$, respectively.

## Conclusions

In summary, we have prepared four new examples of (110)-type LHPs. Formamidinium is shown to template two unusual variants of this structure type; γ-$(FA)_2PbBr_4$ having a 3 × 2 step-like inorganic layer, and $(FA)_{1.5}(AA)_{0.5}PbBr_4$, which exhibits a 3:1 cation ordered 'eclipsed' 2 × 2 structure. The identification of a third polymorph of $(FA)_2PbBr_4$ underlines the rich possibilities of exploring alternative synthetic methods in these systems, which is likely to lead to tailorable modifications to electronic and optical properties, as shown by our preliminary studies above. The introduction of pyrazolium and 1,2,3-triazolium into the family of amines able to direct the formation of (110)-type LHPs reinforces our own observations, supported by other workers[11], that small, rigid disc-shaped amines which are capable of multiple H-bonding interactions are suitable templates for this structural architecture. Observation of a particularly low band gap (2.62 eV) for $(FA)_{1.5}(AA)_{0.5}PbBr_4$ suggests that the 3:1 ordered, eclipsed architecture may favour this particular feature. Further work is required to fully map out the range of possible templating cations, together with the effects of reaction conditions on polymorphism and consequent optimisation of electro-optical properties.

**Table 1.** Crystal and Structure Refinement Data for γ-$(FA)_2PbBr_4$, $(FA)_{1.5}(AA)_{0.5}PbBr_4$, (PY)(GA)$PbBr_4$ and (PY)(TZ)$PbBr_4$.

| | γ-$(FA)_2PbBr_4$ | $(FA)_{1.5}(AA)_{0.5}PbBr_4$ | (PY)(GA)$PbBr_4$ | (PY)(TZ)$PbBr_4$ |
|---|---|---|---|---|
| **Formula** | $C_2H_{10}N_4PbBr_4$ | $C_{2.5}H_{11}N_4PbBr_4$ | $C_4H_{11}N_5PbBr_4$ | $C_5N_5H_9PbBr_4$ |
| **Formula weight** | 616.97 | 623.98 | 655.98 | 665.97 |
| **Colour/Habit** | Colourless/Prism | Yellow/Prism | Colourless/Chip | Colourless/Prism |
| **Crystal size ($mm^3$)** | 0.18 × 0.12 × 0.03 | 0.08 × 0.03 × 0.03 | 0.22 × 0.13 × 0.07 | 0.05 × 0.03 × 0.02 |
| **Temperature (K)** | 93 | 93 | 173 | 173 |
| **Crystal system** | Monoclinic | Monoclinic | Triclinic | Orthorhombic |
| **Space group** | $P2_1/n$ | $P2_1/c$ | $P\bar{1}$ | $Pmc2_1$ |
| ***a* (Å)** | 13.4170(11) | 11.944(4) | 6.0682(5) | 6.0659(3) |
| ***b* (Å)** | 11.8886(10) | 25.414(6) | 9.1499(7) | 13.1562(12) |
| ***c* (Å)** | 23.767(2) | 8.649(3) | 13.2276(10) | 9.3645(10) |
| **α (°)** | | | 92.334(7) | 90 |
| **β (°)** | 102.076(2) | 96.017(8) | 92.316(6) | 90 |
| **γ (°)** | | | 91.902(6) | 90 |
| ***V* ($Å^3$)** | 3707.2(5) | 2610.9(14) | 732.79(10) | 747.32(10) |
| ***Z*** | 12 | 8 | 2 | 2 |
| **$\rho_{calc}$ ($g/cm^3$)** | 3.316 | 3.175 | 2.948 | 2.960 |
| **$\mu$ ($mm^{-1}$)** | 22.546 | 25.130 | 22.393 | 21.961 |
| **F(000)** | 3264 | 2208 | 584 | 592 |
| **Reflns collected** | 39200 | 16295 | 7472 | 9460 |
| **Independent reflns ($R_{int}$)** | 6510 (0.0510) | 4572 (0.0953) | 3328 (0.0961) | 1893 (0.0327) |
| **Goodness of Fit** | 0.959 | 0.934 | 0.911 | 1.026 |

10.1002/ejic.202100433

| | | | | |
|---|---|---|---|---|
| $R_1$ ($I > 2\sigma(I)$) | 0.0201 | 0.046 | 0.0491 | 0.0287 |
| $wR_2$ (all data) | 0.0421 | 0.1095 | 0.1242 | 0.0617 |
| Largest diff. peak/hole (e Å$^{-3}$) | 1.603/-1.980 | 3.357/-2.443 | 4.048/-3.062 | 1.032/-0.963 |

**Table 2.** Selected bond lengths (Å), bond angles (°) and calculated octahedral distortions for γ-$(FA)_2PbBr_4$, $(FA)_{1.5}(AA)_{0.5}PbBr_4$, (PY)(GA)$PbBr_4$ and (PY)(TZ)$PbBr_4$

| | **γ-$(FA)_2PbBr_4$** | | | **$(FA)_{1.5}(AA)_{0.5}PbBr_4$** | |
|---|---|---|---|---|---|
| | Pb1 | Pb2 | Pb3 | Pb1 | Pb2 |
| **Pb-Br (Å)** | 2.9512(6) | 2.8507(5) | 2.8941(5) | 2.9013(12) | 2.8687(12) |
| | 2.9768(5) | 2.8511(5) | 2.9231(6) | 2.9301(13) | 2.9652(14) |
| | 2.9916(5) | 2.9750(5) | 2.9850(5) | 2.9959(13) | 3.0000(14) |
| | 2.9977(5) | 3.0581(5) | 3.0186(5) | 3.0169(14) | 3.0055(13) |
| | 3.0222(6) | 3.2275(5) | 3.0954(6) | 3.0423(12) | 3.0299(13) |
| | 3.0412(5) | 3.2622(5) | 3.1143(5) | 3.0748(13) | 3.1195(13) |
| **Pb-Br-Pb (°)** | 166.06(1) | 173.32(2) | 163.24(2) | 163.37(4) | 163.37(4) |
| | 173.32(2) | 160.71(2) | 163.98(2) | 173.20(5) | 173.20(5) |
| | 163.24(2) | | | 173.73(4) | 169.20(6) |
| **Br-Pb-Br range (°)** | 85.87(2)-95.90(2) | 82.58(1)-98.46(1) | 86.67(1)-94.19(1) | 84.65(3)-99.54(3) | 86.48(3)-94.91(3) |
| **Δd (×10⁻⁴)** | 0.95 | 29.00 | 7.33 | 4.10 | 6.24 |
| **σ²** | 7.51 | 25.27 | 7.16 | 20.67 | 8.47 |

| | **(PY)(GA)$PbBr_4$** | **(PY)(TZ)$PbBr_4$** |
|---|---|---|
| **Pb-Br (Å)** | 2.8717(13) | 2.891(6) |
| | 2.9083(13) | 2.894(6) |
| | 2.9831(11) | 3.0336(2) |
| | 3.0904(11) | 3.0336(2) |
| | 3.1012(5) | 3.124(8) |
| | 3.1229(5) | 3.131(8) |
| **Pb-Br-Pb (°)** | 175.21(5) | 177.54(6) |
| | 180 | 179.2(3) |
| **Br-Pb-Br range (°)** | 85.71(2)-98.58(2) | 86.9(2)-96.95(2) |
| **Δd (×10⁻⁴)** | 10.58 | 10.22 |
| **σ²** | 14.88 | 6.49 |

## Experimental Section

### Synthesis

Formamidine acetate ($CH_4N_2 \cdot CH_3COOH$, 99%), acetamidine hydrochloride, ($C_2H_6N_2 \cdot HCl$, 97%), pyrazole ($C_3H_4N_2$) and 1,2,3-triazole ($C_2H_3N_3$, 99%), lead (II) bromide ($PbBr_2$, ≥98%) and hydrobromic acid (HBr, 48%, w/w aqueous solution) were purchased from Alfa Aesar. Guanidinium carbonate ($C_2H_{10}N_6H_2CO_3$, 99%) and diethyl ether ($(C_2H_5)_2O$, 99.5%) were purchased from Sigma Aldrich. All chemicals were directly used without further purification.

The four title compounds were all crystallised from concentrated hydrobromic acid by the slow evaporation method.

**$(FA)_2PbBr_4$** ($C_2H_{10}N_4PbBr_4$), the reactants formamidine acetate (2498 mg, 24 mmol) and $PbBr_2$ (734 mg, 2 mmol) were dissolved in concentrated HBr (8 mL) with moderate heating. By naturally cooling the solvent for a few hours or overnight, pale yellow, needle-shaped crystals were obtained. These crystals were then collected by filtering and washed with diethyl ether (yield 36% based on $PbBr_2$). Elemental analysis: (Analysis Found (%) for $C_2H_{10}N_4PbBr_4$: C, 3.93; H, 1.62; N, 9.16. Calculated: C, 3.89; H, 1.63; N, 9.08).

**$(FA)_{1.5}(AA)_{0.5}PbBr_4$** ($C_{2.5}H_{11}N_4PbBr_4$), the reactants formamidine acetate (1249 mg, 12 mmol), acetamidine hydrochloride (1134 mg, 12 mmol) and $PbBr_2$ (734 mg, 2 mmol) were dissolved in concentrated HBr (10 mL) with moderate heating. By naturally cooling the solvent for a few hours or overnight, yellow, needle-shaped crystals were obtained. These crystals were then collected by filtering and washed with acetone (yield 41% based on $PbBr_2$). Elemental analysis: (Analysis Found (%) for $C_{2.5}H_{11}N_4PbBr_4$: C, 4.72; H, 1.62; N, 8.88. Calculated: C, 4.81; H, 1.78; N, 8.98).

**[PY][GA]$PbBr_4$** ($C_4H_{11}N_5PbBr_4$), stoichiometric amounts of pyrazole (136 mg, 2 mmol), guanidinium carbonate (180 mg, 1 mmol) and $PbBr_2$ (737 mg, 2 mmol) were dissolved in conc. HBr (3 mL) with moderate heating. By cooling for a few hours, colourless cuboid-shaped crystals were obtained. These were filtered and washed with diethyl ether. Elemental analysis: (Anal. Calc. (%) for $C_4H_{11}N_5PbBr_4$: C, 7.32; H, 1.69; N, 10.68. Found: C, 7.66; H, 1.61; N, 10.29).

**[PY][TZ]$PbBr_4$** ($C_5H_9N_5PbBr_4$), stoichiometric amounts of pyrazole (136 mg, 2 mmol), 1,2,3-triazole (138 mg, 2 mmol) and $PbBr_2$ (737 mg, 2 mmol) were dissolved in conc. HBr (3 mL) with moderate heating. By cooling for a few hours, colourless, cuboid-shaped crystals were

obtained. These were filtered and washed with diethyl ether. While the simulated XRD pattern from the single crystal structure suggests the sample is phase pure, elemental analysis indicates that both the % of both C and N are lower than expected. This may indicate some sample decomposition. Elemental analysis: (Anal. Calc. (%) for $C_5H_9N_5PbBr_4$: C, 9.02; H, 1.36; N, 10.52. Found: C, 8.16; H, 1.05; N, 8.16). The elemental analysis of [PY][TZ]$PbBr_4$ cannot be rationalised by variation of either [PY] or [TZ] suggesting that some sample degradation may have occurred although the XRD pattern suggests that on synthesis the sample is pure.

**Characterisation**

Single crystal X-ray diffraction data were collected on a Rigaku XtaLAB P200 diffractometer at 93 K for $(FA)_2PbBr_4$, $(FA)_{1.5}(AA)_{0.5}PbBr_4$ and on a Rigaku SCX Mini X-ray diffractometer at 173 K for [PY][GA]$PbBr_4$ and [PY][TZ]$PbBr_4$ using Mo-$K_\alpha$ ($\lambda$ = 0.71075 Å) radiation. The data were recorded by Rigaku CrystalClear software.[32] Crystal structures were solved by direct methods using structure solution program SHELXT,[33] with refinements of full-matrix least-squares on $F^2$ by using SHELXL-2018/3[34] incorporated in the WinGX software.[34] The corrections for absorption were conducted empirically from equivalent reflections according to multi-scans by using the CrystalClear software.[32] All the hydrogen atoms were treated as rigid atoms, and all non-H atoms were refined anisotropically. Powder X-ray diffraction data were collected on a PANalytical EMPYREAN diffractometer using Cu $K_{\alpha1}$ ($\lambda$ = 1.5406 Å) radiation in the range of 5 to 50° to confirm the purity of each sample. Ambient temperature solid UV-Vis absorbance spectra were collected on a JASCO-V550 ultraviolet–visible spectrophotometer with the wavelength range at 200 nm to 900 nm.

**CCDC Reference numbers:** 2064367 for $(FA)_{1.5}(AA)_{0.5}PbBr_4$ (93 K) 2064368 for (PY)(GA)$PbBr_4$ (298 K), 2064369 for (PY)(TZ)$PbBr_4$ (173 K), 2064370 for (PY)(GA)$PbBr_4$ (173 K) and 2064371 for $\gamma$-$(FA)_2PbBr_4$ (93 K)

**Acknowledgements**

We acknowledge support from the University of St Andrews, the China Scholarship Council (studentship to YYG) and Leverhulme Trust (RPG-2018-065).

**Keywords**

Crystal engineering

Halides

10.1002/ejic.202100433

Layered compounds

Perovskite phases

Polymorphism

10.1002/ejic.202100433

## Graphical Abstract

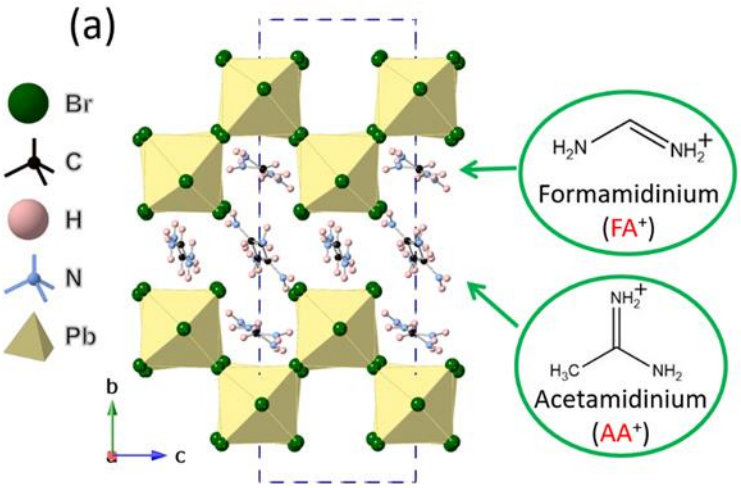


Four new (110)-type lead bromide perovskites are presented, including new examples of 3:1 cation ordering and 3 x 2 step-like structures. The structural diversity observed here reflects subtle control of polymorphism in these layered systems containing small, rigid amines with multiple hydrogen-bonding opportunities.

## References


1 X. Li, J. Hoffman, W. Ke, M. Chen, H. Tsai, W. Nie, A. D. Mohite, M. Kepenekian, C. Katan, J. Even, M. R. Wasielewski, C. C. Stoumpos, M. G. Kanatzidis, *J. Am. Chem. Soc.* **2018**, *140*, 12226–12238.

2 L. Mao, W. Ke, L. Pedesseau, Y. Wu, C. Katan, J. Even, M. R. Wasielewski, C. C. Stoumpos, M. G. Kanatzidis, *J. Am. Chem. Soc.* **2018**, *140*, 3775–3783.

3 M. D. Smith, B. A. Connor, H. I. Karunadasa, *Chem. Rev.* **2019**, *119*, 3104–3139.

4 W. S. Yang, J. H. Noh, N. J. Jeon, Y. C. Kim, S. Ryu, J. Seo, S. II Seok, *Science* **2015**, *348*, 1234–1237.

5 A. Perumal, S. Shendre, M. Li, Y. K. E. Tay, V. K. Sharma, S. Chen, Z. Wei, Q. Liu, Y. Gao, P. J. S. Buenconsejo, S. T. Tan, C. L. Gan, Q. Xiong, T. C. Sum, H. V. Demir, *Sci. Rep.* **2016**, *6*, 1–10.

6 L. Protesescu, S. Yakunin, M. I. Bodnarchuk, F. Bertolotti, N. Masciocchi, A. Guagliardi, M. V. Kovalenko, *J. Am. Chem. Soc.* **2016**, *138*, 14202–14205.

7 B. A. Rosales, L. E. Mundt, T. G. Allen, D. T. Moore, K. J. Prince, C. A. Wolden, G. Rumbles, L. T. Schelhas, L. M. Wheeler, *Nat. Commun.* **2020**, *11*, 1–12.

8 M. C. Gélvez-Rueda, P. Ahlawat, L. Merten, F. Jahanbakhshi, M. Mladenović, A. Hinderhofer, M. I. Dar, Y. Li, A. Dučinskas, B. Carlsen, W. Tress, A. Ummadisingu, S. M. Zakeeruddin, F. Schreiber, A. Hagfeldt, U. Rothlisberger, F. C. Grozema, J. V. Milić, M. Graetzel, *Adv. Funct. Mater.* **2020**, *30*, 1–9.

9 M. B. H. Salah, N. Mercier, M. Allain, N. Zouari, U. Giovanella, C. Botta, *Eur. J. Inorg. Chem.* **2019**, 4527–4531.

10 O. Nazarenko, M. R. Kotyrba, S. Yakunin, M. Aebli, G. Rainò, B. M. Benin, M. Wörle, M. V. Kovalenko, *J. Am. Chem. Soc.* **2018**, *140*, 3850–3853.

11 S. A. Fateev, A. A. Petrov, E. I. Marchenko, Y. V Zubavichus, V. N. Khrustalev, A. V Petrov, S. M. Aksenov, E. A. Goodilin, A. B. Tarasov, *Chem. Mater.*, **2021**, *33*, 1900-1907.

12 J. A. McNulty, P. Lightfoot, *IUCrJ*, **2021**, 8, 485-513.

13 E. I. Marchenko, S. A. Fateev, A. A. Petrov, V. V. Korolev, A. Mitrofanov, A. V. Petrov,

E. A. Goodilin, A. B. Tarasov, *Chem. Mater.* **2020**, *32*, 7383–7388.

14 C. Katan, N. Mercier, J. Even, *Chem. Rev.* **2019**, *119*, 3140–3192.

15 Y.-Y. Guo, J. A. McNulty, N. A. Mica, I. D. W. Samuel, A. M. Z. Slawin, M. Bühl, P. Lightfoot, *Chem. Commun.* **2019**, *55*, 9935–9938.

16 Y.-Y. Guo, L. Yang, S. Biberger, J. A. McNulty, T. Li, K. Schötz, F. Panzer, P. Lightfoot, *Inorg. Chem.* **2020**, *59*, 12858–12866.

17 A. R. Rae Smith, A. K. Cheetham, *J. Solid State Chem.* **1979**, *30*, 345–352.

18 A. K. Cochrane, M. Telfer, C. A. L. Dixon, W. Zhang, P. S. Halasyamani, E. Bousquet, P. Lightfoot, *Chem. Commun.* **2016**, *52*, 10980–10983.

19 M. Daub, C. Haber, H. Hillebrecht, *Eur. J. Inorg. Chem.* **2017**, 1120–1126.

20 D. B. Mitzi, S. Wang, C. A. Feild, C. A. Chess, A. M. Guloy, *Science* **1995**, *267*, 1473–1476.

21 M. H. Tremblay, F. Thouin, J. Leisen, J. Bacsa, A. R. Srimath Kandada, J. M. Hoffman, M. G. Kanatzidis, A. D. Mohite, C. Silva, S. Barlow, S. R. Marder, *J. Am. Chem. Soc.* **2019**, *141*, 4521–4525.

22 J. A. McNulty, P. Lightfoot, *Chem. Commun.* **2020**, *56*, 4543–4546.

23 J. A. McNulty, A. M. Z. Slawin, P. Lightfoot, *Dalton Trans.* **2020**, *49*, 15171–15174.

24 C. J. Que, C. J. Mo, Z. Q. Li, G. L. Zhang, Q. Y. Zhu, J. Dai, *Inorg. Chem.* **2017**, *56*, 2467–2472.

25 C. J. Adams, M. A. Kurawa, A. G. Orpen, *Inorg. Chem.* **2010**, *49*, 10475–10485.

26 E. R. Dohner, A. Jaffe, L. R. Bradshaw, H. I. Karunadasa, *J. Am. Chem. Soc.* **2014**, *136*, 13154–13157.

27 R. Gautier, F. Massuyeau, G. Galnon and M. Paris, *Adv. Mater.* **2019**, *31*, 1807383.

28 E. R. Dohner, E. T. Hoke, H. I. Karunadasa, *J. Am. Chem. Soc.* **2014**, *136*, 1718–1721.

29 Z. Cheng, J. Lin, *CrystEngComm* **2010**, *12*, 2646–2662.

30 K. Pradeesh, K. Nageswara Rao, G. Vijaya Prakash, *J. Appl. Phys.* **2013**, *113*, 083523.

31 B. Febriansyah, D. Giovanni, S. Ramesh, T. M. Koh, Y. Li, T. C. Sum, N. Mathews, J.

England, *J. Mater. Chem. C* **2020**, *8*, 889–893.

32 *CrystalClear - SM Expert* v2.1. Rigaku Americas, *The Woodlands, Texas, USA*, and Rigaku Corporation, *Tokyo, Japan*, **2015**.

33 G. M. Sheldrick, *Acta Cryst. C* **2015**, *71*, 3–8.

34 L. J. Farrugia, *J. Appl. Crystallogr.* **2012**, *45*, 849–854.